This is a repository copy of *Amylose recognition and ring-size determination of amylomaltase*.

White Rose Research Online URL for this paper:
https://eprints.whiterose.ac.uk/112084/

Version: Published Version

Amylose recognition and ring-size determination of amylomaltase

Christian Roth,[1,2]*[†] Nicole Weizenmann,[3†] Nicola Bexten,[4‡] Wolfram Saenger,[4]
Wolfgang Zimmermann,[3]* Timm Maier,[5]* Norbert Sträter[1]*

Starch is a major carbon and energy source throughout all kingdoms of life. It consists of two carbohydrate polymers, branched amylopectin and linear amylose, which are sparingly soluble in water. Hence, the enzymatic breakdown by glycoside hydrolases (GHs) is of great biological and societal importance. Amylomaltases (AMs) are GHs specialized in the hydrolysis of α-1,4–linked sugar chains such as amylose. They are able to catalyze an intramolecular transglycosylation of a bound sugar chain yielding polymeric sugar rings, the cycloamyloses (CAs), consisting of 20 to 100 glucose units. Despite a wealth of data on short oligosaccharide binding to GHs, no structural evidence is available for their interaction with polymeric substrates that better represent the natural polysaccharide. We have determined the crystal structure of *Thermus aquaticus* AM in complex with a 34-meric CA—one of the largest carbohydrates resolved by x-ray crystallography and a mimic of the natural polymeric amylose substrate. In total, 15 glucose residues interact with the protein in an extended crevice with a length of more than 40 Å. A modified succinimide, derived from aspartate, mediates protein-sugar interactions, suggesting a biological role for this nonstandard amino acid. The structure, together with functional assays, provides unique insights into the interaction of GHs with their polymeric substrate and reveals a molecular ruler mechanism for minimal ring-size determination of CA products.

INTRODUCTION

Polysaccharides with low water solubility, such as starch in plants and glycogen in animals and prokaryotes, are the main carbon and energy source of life. The cleavage of these polymeric substrates is achieved by enzymes of the families of glycoside hydrolases (GHs) and transglycosylases or polysaccharide phosphorylases. Amylomaltases (AMs) are classified as bacterial intracellular hydrolases of the GH77 family of carbohydrate-active enzymes (*1*). They are involved in glycogen degradation as well as maltose metabolism and are related to the disproportionating enzymes of plant plastids (*2*). AMs catalyze the cleavage of an α-1,4-glucan, resulting in the formation of a glycosyl-enzyme intermediate in the first part of the catalytic cycle. Subsequently, the intermediate is broken down via reaction with an acceptor, which may be another α-1,4-glucan, glucose, or water, with the latter resulting in hydrolysis (Fig. 1).

If the nonreducing end of the bound glucan chain acts as an acceptor, intramolecular transfer results in a cyclization that yields cycloamyloses (CAs) with a degree of polymerization (dp) of 20 and higher (*3*). CAs are a longer form of the more common α-, β-, or γ-cyclodextrins (CDs; with ring sizes of six, seven, or eight glucoses, respectively). Similar to CDs, the larger CAs have a hydrophobic inner surface, whereas their outside is hydrophilic. In contrast to the ring-shaped CDs, the CAs adopt more complex, folded structures, but they also form inclusion complexes with water, ions, or hydrophobic compounds, such as long-chain fatty acids (*4*–*6*), and show promising chaperone activity in the course of protein refolding (*7*). However, difficulties in the commercial-scale selective production of CAs of distinct ring size currently still limit their industrial applicability compared to CDs.

AMs comprise a catalytic core (β/α)$_8$-barrel domain (A), three inserted subdomains (B1, B2, and B3), and a loop covering the active center, as shown by the crystal structure of the 55-kDa *Thermus aquaticus* AM (TaqAM) (Fig. 2A). The catalytic mechanism of AMs was revealed by crystallographic snapshots of *Thermus thermophilus* AM with a covalently bound intermediate and an acceptor analog in subsites −1 and +1, respectively (*8*). AMs do not contain canonical carbohydrate-binding domains or motifs, but a cocrystal structure with the inhibitor acarbose has identified a secondary carbohydrate-binding site between the unique B2 domain and the core (β/α)$_8$-barrel in addition to the primary binding region around the active site comprising D293, E340, and D395 (*9*). On the basis of all available structures and biochemical data, a continuous binding site for up to seven consecutive carbohydrate moieties, −4 to +3 with respect to the enzymatic cleavage site, has been postulated for AMs (*10*). Further interactions with native polymeric substrates have only been depicted in conceptual models (*9*), whereas the characteristic interaction of these enzymes with CAs or polymeric substrates remains unknown. Here, we report the crystal structure of TaqAM in complex with a 34-meric CA (CA34), which, in combination with a series of catalytic assays, reveals the mechanisms of substrate recognition and CA ring-size determination by AMs as well as a contribution of a nonstandard aspartate-derived amino acid, succinimide, to carbohydrate interaction. The observed conformation of CA34 in the substrate crevice provides a model of the interaction of AMs with the helical amylose of starch.

RESULTS AND DISCUSSION

The cocrystal structure of CA34 bound to TaqAMv shows a continuous binding path for 16 glucose units

On the basis of the available structural as well as functional data for AMs and mutagenesis data on the CD glucanotransferase from *Bacillus circulans* strain 251, we designed the active site double mutant D293A/D395N to obtain an inactive TaqAM variant (*11*), TaqAMv.

[1]Institut für Bioanalytische Chemie, Universität Leipzig, Deutscher Platz 5, 04103 Leipzig, Germany. [2]Department of Chemistry, University of York, Heslington, York, YO10 5DD, U.K. [3]Institut für Biochemie, Universität Leipzig, Johannisallee 21-23, 04103 Leipzig, Germany. [4]Institut für Chemie-Kristallographie, Freie Universität Berlin, Takustrasse 6, 14195 Berlin, Germany. [5]Biozentrum, Universität Basel, Biozentrum, Klingelbergstrasse 50/70, CH-4056 Basel, Switzerland.
*Corresponding author. Email: christian.roth@york.ac.uk (C.R.); wolfgang.zimmermann@uni-leipzig.de (W.Z.); timm.maier@unibas.ch (T.M.); strater@bbz.uni-leipzig.de (N.S.)
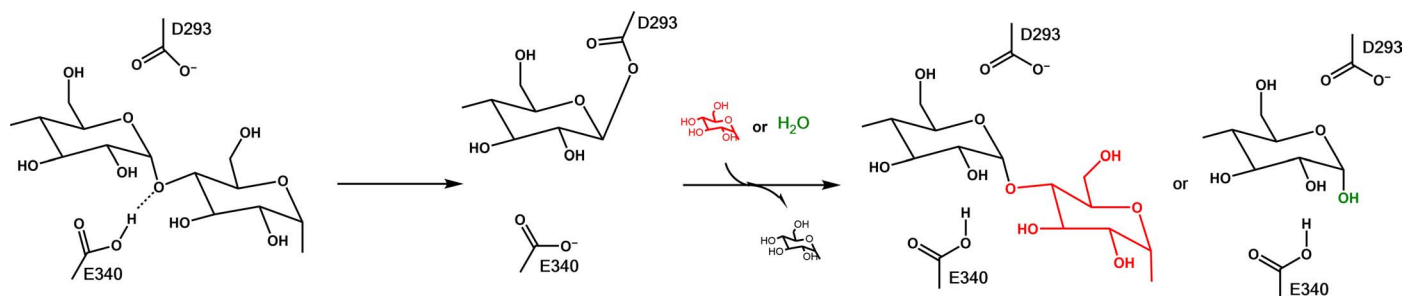†These authors contributed equally to this work.
‡Deceased.

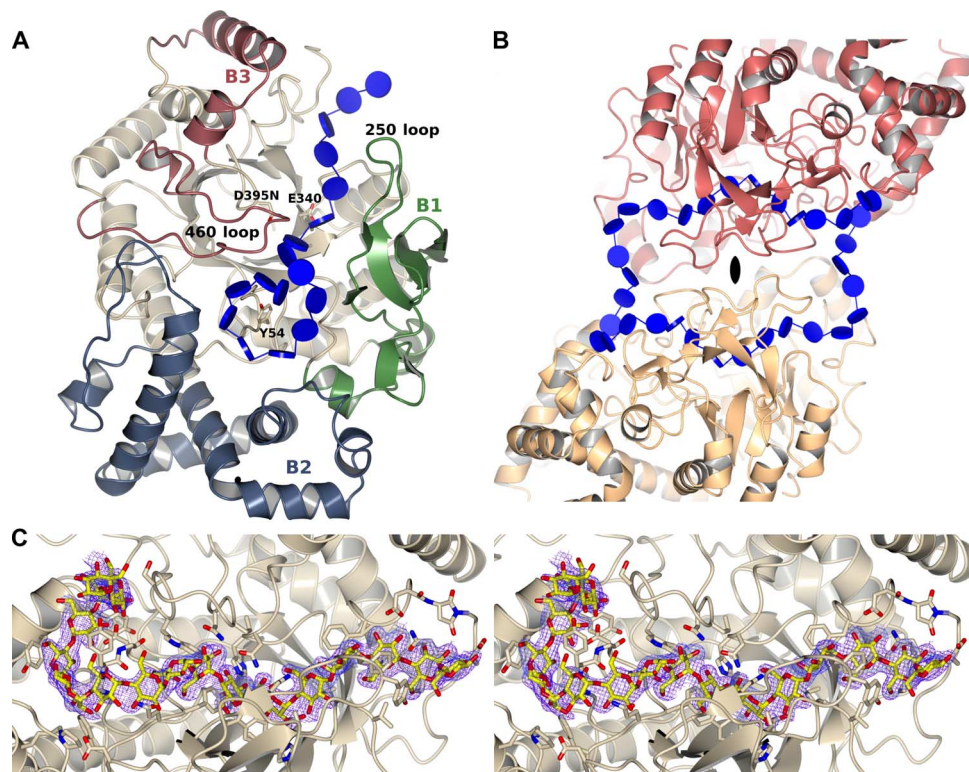**Fig. 1. Reaction mechanism of TaqAM leading to transglycosylation or hydrolysis.**

Fig. 2. Cocrystal structure of CA34 bound to TaqAM. (**A**) Overview of the TaqAM fold. In addition to the $(\beta/\alpha)_8$-barrel, three subdomains (B1, B2, and B3) are present. (**B**) Representation of the crystallographic dimer bridged by the bound CA34 (shown as blue glycoblock representation). The symmetry-related monomers are shown in red and beige. (**C**) Binding of CA residues 1 to 16 to one monomer of TaqAM shown in stereo. The corresponding $2mF_o - DF_c$ electron density around the CA after refinement is contoured at 1σ.

Crystals of TaqAMv in the presence of a CA mixture containing CA22 to CA45 were obtained in space group I422, distinct from previously reported crystals forms of TaqAM (2, 8, 9), and diffract to 1.7 Å resolution. The crystallographic asymmetric unit contains one TaqAMv molecule and half of the CA34. The structure of TaqAMv closely resembles the structures of the apo- and acarbose-bound TaqAM with main-chain root mean square deviations of 0.5 and 0.6 Å, respectively. Inside and beyond the active site of TaqAMv, a bound CA ligand is observed (Fig. 2C and fig. S1), which interacts with one AM molecule and further continues toward a symmetry-related protein molecule in the crystal with unambiguous electron density for all glucose moieties.

The two symmetry-related CA halves are joined to form a CA34 ring (Fig. 2B), which connects the two TaqAMv monomers such that a twofold crystallographic symmetry axis runs through the center of the bound CA34 nearly perpendicular to the active site crevice. Appar-

ently, crystallization selectively occurred for CA34 in the presence of an excess of CA of other ring sizes in the CA pool used for cocrystallization. For the interaction with their substrates, many GHs rely on noncatalytic carbohydrate-binding domains or secondary binding sites outside the active site region (12–14). The importance of such substrate recognition sites is demonstrated by the fact that mutations in corresponding regions lead to functionally impaired variants, which may lead to severe diseases such as type III glycogen storage disease (15).

Soaking of TaqAMv with the inhibitor acarbose had previously revealed a secondary carbohydrate-binding site around Y54 and Y101 between the $(\beta/\alpha)_8$-barrel domain A and the unique B2 domain (9). Further enzymatic analysis confirmed the functional relevance of this secondary binding site and led to the proposition of an extended binding site for up to seven carbohydrate moieties (10). However, the
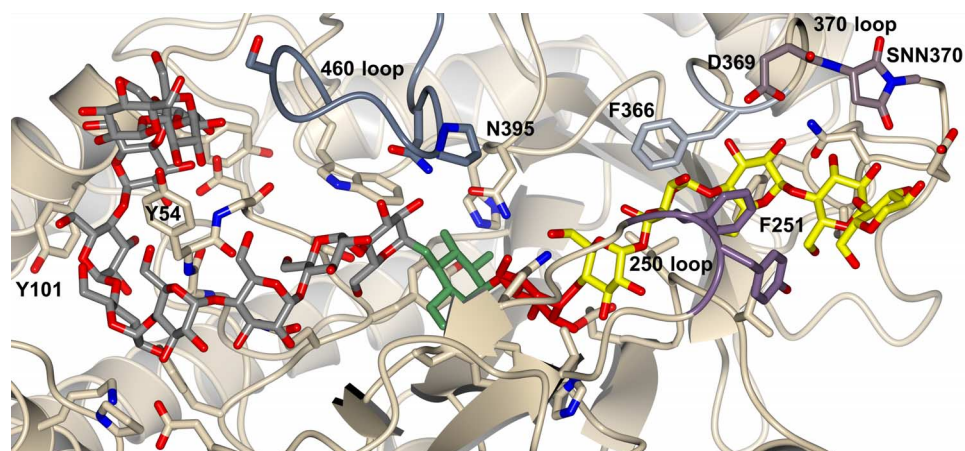
Fig. 3. Interactions of CA34 with TaqAM. Binding of CA residues 1 to 16 to one monomer of TaqAM. Glc–1 (green) and the preceding residues of the donor site are shown on the left side with the carbon in gray, whereas Glc+1 (red) and the following residues in the acceptor binding sites are on the right side with the carbon in yellow. The 250 loop (amino acids 247 to 255) is in purple, the 370 loop (amino acids 368 to 372) is in dark pink, the 460 loop (amino acids 458 to 472) is in dark blue, F366 (part of the acceptor sugar tong) is in light blue, whereas the remaining molecule is in beige. These loops are assumed to be of importance for AM function (2).

Table 1. Geometric parameter for the carbohydrate units of CA34. Torsion angles that deviate by >10° from those observed in V-amylose and distances O3(n)–O2(n + 1) that are too long for a hydrogen bonding interaction are underlined to indicate conformational changes of the CA34 molecule due to binding to AM. Residues −7 to −9, which form the core of the helical region wrapping around Y54, most closely correspond to the V-amylose helix conformation as characterized by the torsion angles φ between 91° and 115° as well as ψ between 97° and 131° and by the presence of O3(n)–O2(n + 1) hydrogen bonds as observed in the helical regions of the crystal structure of CA26 (36).

Sugar	Residue	B factor [Å²]	Φ [°] O5(n)–C1(n)–O4(n − 1)–C4(n − 1)	Ψ [°] C1(n)–O4(n − 1)–C4(n − 1)–C3(n − 1)	χ [°] (O5–C5–C6–O6)	Distance [Å] O3(n)–O2(n + 1)
1	+6	117.9	111.6	<u>65.94</u>	−66.6	3.07
2	+5	44.9	99.7	99.9	−59.3	2.94
3	+4	43.0	104.5	98.1	−69.1	<u>4.04</u>
4	+3	78.9	<u>73.8</u>	90.8	−77.1	<u>4.36</u>
5	+2	60.5	<u>60.5</u>	<u>83.6</u>	−55.9	<u>4.06</u>
6	+1	43.9	<u>65.2</u>	90.1	61.3	<u>4.21</u>
7	−1	63.4	<u>59.1</u>	88.3	49.8	3.80
8	−2	71.8	<u>74.9</u>	89.1	<u>29.9</u>	3.60
9	−3	112.7	81.9	84.6	55.6	<u>4.72</u>
10	−4	124.8	<u>44.5</u>	<u>72.3</u>	65.7	<u>2.26</u>
11	−5	148.7	<u>141.1</u>	121.0	<u>38.7</u>	3.56
12	−6	74.3	<u>86.6</u>	83.7	<u>163.3</u>	2.84
13	−7	76.8	114.5	116.4	55.0	2.85
14	−8	97.6	110.4	95.4	50.3	2.59
15	−9	102.6	120.5	123.8	<u>42.4</u>	<u>3.72</u>
16	−10	126.1	84.7	83.4	92.2	<u>4.47</u>
17	−11	130.8	<u>60.9</u>	<u>67.0</u>	<u>148.4</u>	3.51

current structure shows a considerably more extended substrate-binding site that accommodates 16 glucose units and is formed by the core (β/α)₈-barrel domain with supporting residues from all subdomains (Fig. 3).

All glucose units adopt the $^4C_1$ chair conformation (Table 1). In the active site, glucose Glc−1 interacts with H394 and N395 (the mutated native D395), whereas Glc+1 interacts with E340 as well as N256, representing the ground state of the active site. F251 from subdomain
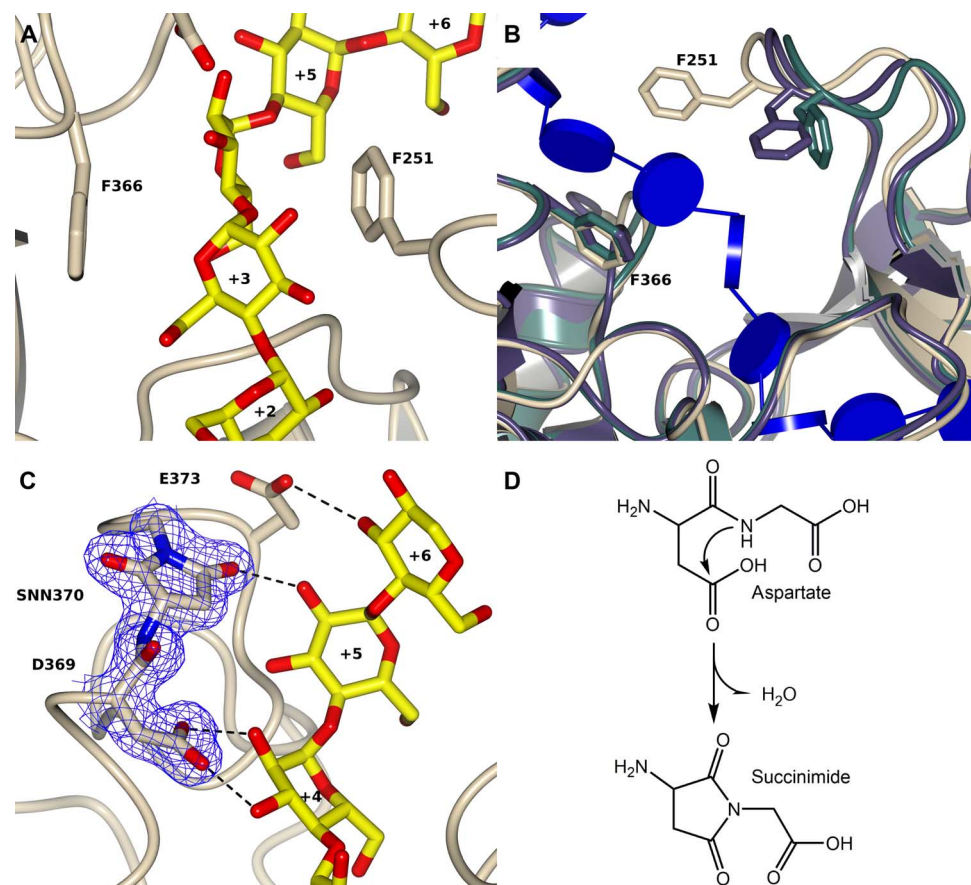
Fig. 4. Sugar tongs and succinimide in CA binding. (A) Close-up of the acceptor sugar tong formed by F251 and F366. **(B)** Movement of the 250 loop in response to inhibitor or substrate binding. The unliganded enzyme is in dark green [Protein Data Bank (PDB) ID, 1CWY], the acarbose complex is in purple (PDB ID, 1ESW), and the CA34-bound structure is in beige. The bound CA34 is shown in glycoblocks for better orientation, and the tong-forming residues are depicted in stick representation. **(C)** The imide formed by D370. The imide and D369 are shown in stick representation with the corresponding $2mF_o − DF_c$ density contoured at 1.5σ (blue). The hydrogen bond of the imide with O2 of Glc+5 is shown as dashed lines. The remaining hydrogen bond contacts on the acceptor site with D369 and E373 are shown as well. **(D)** Schematic representation of the imide formation. The imide forms through a nucleophilic attack of the peptide backbone nitrogen on the carboxyl carbon of the preceding aspartate. The subsequent dehydration leads to a stable five-membered ring structure.

Table 2. Enzymatic activities of AM and mutants thereof, divided into cyclization, disproportionation, coupling, and hydrolysis.

AM	Cyclization		Disproportionation		Coupling		Hydrolysis	
	U/mg	Relative (%)	U/mg	Relative (%)	U/mg	Relative (%)	U/mg	Relative (%)
Wild type	0.317	100	1188	100	0.316	100	0.308	100
Y54G	0.057	18	66	5.6	0.190	60	0.101	33
S57R	0.003	1	5	0.4	0.001	0.3	0.037	12
Y101G	0.011	3.5	139	12	0.006	1.9	0.164	53
+SY^{250}F^{251}+S	0.0002	0.1	10	0.8	0.002	0.6	0.125	41
D370S	0.169	53	1340	113	0.125	40	0.414	134

B1 and F366 from the $(\beta/\alpha)_8$-barrel form a sugar tong interacting hydrophobically with Glc+3 (Fig. 4A). The 250 loop (amino acids 247 to 255) adopts different conformations in the unliganded, acarbose-bound, and CA-bound structures (Fig. 4B); this loop has been hypothesized to play a role in the unusually high transglycosylation activity for GH77 enzymes (*2*, *9*).

We mutated the 250 loop to prevent the proper formation of that sugar tong. An elongation of the loop by insertion of two serines

Table 3. Kinetic parameters for the cyclization, disproportionation, and coupling reactions catalyzed by the wild-type and mutated AMs.

AM	Cyclization			Disproportionation			Coupling		
	K_m pea starch (mM)	k_{cat} (s^{-1})	k_{cat}/K_m (s^{-1} mM^{-1})	K_m maltotriose (mM)	k_{cat} (s^{-1})	k_{cat}/K_m (s^{-1} mM^{-1})	K_m CD$_{25}$ (mM)	k_{cat} (s^{-1})	k_{cat}/k (s^{-1} mM^{-1})
Wild type	$3.25 \times 10^{-6} \pm 4 \times 10^{-7}$	2.0×10^{-5}	6.15	$2.48 \times 10^{-2} \pm 2 \times 10^{-3}$	9.8×10^{-2}	3.95	$2.48 \times 10^{-3} \pm 2 \times 10^{-4}$	8.2×10^{-3}	3.31
Y54G	$1.53 \times 10^{-6} \pm 2 \times 10^{-7}$	1.2×10^{-6}	0.78	$1.41 \times 10^{-2} \pm 1 \times 10^{-3}$	1.6×10^{-3}	0.11	$3.74 \times 10^{-3} \pm 2 \times 10^{-4}$	4.5×10^{-3}	1.20
S57R	$2.86 \times 10^{-6} \pm 5 \times 10^{-7}$	2.1×10^{-8}	0.0073	$1.75 \times 10^{-2} \pm 2 \times 10^{-3}$	1.0×10^{-4}	0.006	$6.69 \times 10^{-3} \pm 2 \times 10^{-4}$	3.0×10^{-5}	0.005
Y101G	$1.13 \times 10^{-5} \pm 4 \times 10^{-6}$	2.0×10^{-7}	0.018	$2.70 \times 10^{-2} \pm 3 \times 10^{-3}$	1.0×10^{-2}	0.37	$4.80 \times 10^{-2} \pm 9 \times 10^{-4}$	5.5×10^{-3}	0.12
+SY^{250}F^{251}+S	$5.68 \times 10^{-6} \pm 4 \times 10^{-7}$	5.1×10^{-6}	0.90	$1.03 \times 10^{-2} \pm 1 \times 10^{-3}$	6.6×10^{-3}	0.64	$2.86 \times 10^{-3} \pm 2 \times 10^{-4}$	1.0×10^{-5}	0.004
D370S	$5.69 \times 10^{-6} \pm 2 \times 10^{-6}$	2.8×10^{-5}	4.92	$1.61 \times 10^{-2} \pm 5 \times 10^{-3}$	8.9×10^{-2}	5.53	$7.27 \times 10^{-3} \pm 6 \times 10^{-4}$	6.2×10^{-3}	0.85

(+SY^{250}F^{251}+S) strongly reduces the enzymatic activity (Tables 2 and 3). The most pronounced effects are observed for reactions involving acceptor sugars, confirming that the acceptor sugar tong is important for the unusual high transglycosylation activity in the GH77 family. A similar conclusion was drawn on the basis of a complex of *Arabidopsis* plastidial disproportionating enzyme (DPE1) with acarviostatin (16). The remaining acceptor binding sites in TaqAMv are predominantly formed by the 370 loop (amino acids 368 to 372) (Fig. 3). Within this loop, residues D369, D370 (modified to SNN370, see below), and E373 form hydrogen bonds with Glc+4, Glc+5, and Glc+6, respectively.

A succinimide dehydration product is involved in carbohydrate interactions

Residues D370 and G371 of AM form a succinimide dehydration product (SNN370) (Fig. 4, C and D). This unusual posttranslational modification in AM was previously interpreted as an artifact of high temperature during the purification procedure (8). However, the imide formation is observed in all published structures from AMs of different organisms (8). Furthermore, the applied temperature during preparation of the enzyme resembles the growth optimum and the environmental conditions for the source bacterium, *T. aquaticus*. Previously, imides have been described as unstable intermediates in the formation of isoaspartate within labile, flexible peptide sequences (8, 17, 18). Such nonenzymatic posttranslational modification occurs in vivo as well as in vitro under physiological conditions (19) and has been reported for several proteins like the β-amyloid peptide (20), α-A– and B-crystallin (21, 22), hen egg-white lysozyme (18), and ribonuclease U2B (19). Isoaspartate formation has been suggested to play a role in age-dependent protein inactivation (18), and the importance of a repair enzyme for the reversal of isoaspartate formation (the L-isoaspartate methyltransferase) has been demonstrated in knockout mice (23). To date, only two proteins [MurA (24) and ribosomal protein S11 (25)] are known to contain substantial amounts of isoaspartate in vivo; however, the functional role of isoaspartate remains unknown. In contrast, the imide in TaqAMv directly contributes to the formation of the Glc+5 acceptor binding site and accepts a hydrogen bond from O2–H of Glc+5 (Fig. 4), whereas the side chain of the nonmodified aspartate residue would cause a steric clash with Glc+5 of the glycan chain.

The contribution of the imide formation to AM activity is confirmed by the reduced activity of a D370S variant (Table 2) toward long-chain substrates. In particular, the binding of larger substrates is strongly affected, reflected in the huge increase in the K_M value for the cyclization
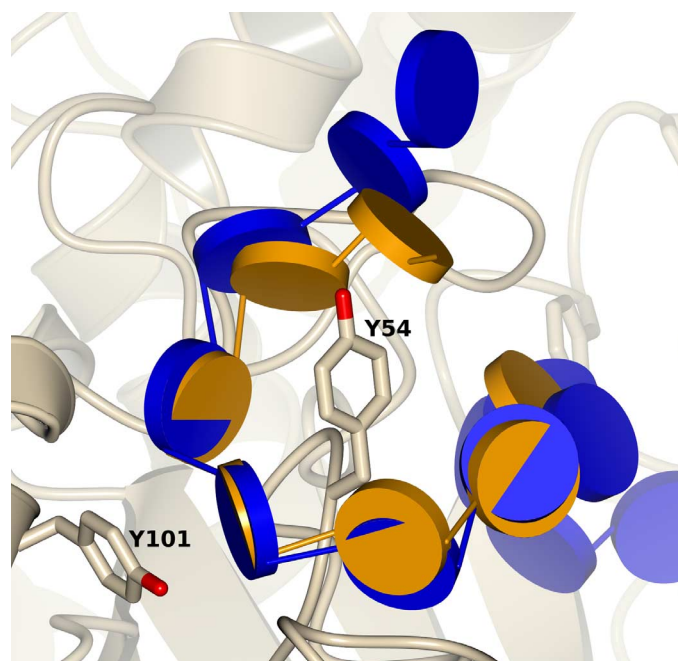

Fig. 5. CA34 mimics amylose binding in the secondary binding site. Close-up of the secondary binding site of AM with bound CA34 shown in blue glycoblocks around Y54. Overlaid in orange is a part of the helix of the crystallized CA26 (PDB ID, 1C58), which resembles the helical structure of V-amylose (35). The two sugar chains have a similar helical conformation, revealing that CA34 in this binding site adopts a conformation, which resembles the low-energy conformation of the free amylose substrate.

and coupling activity (Table 3). Although the seryl oxygen could still form hydrogen bonds to the amylose chain, it cannot replace the imide in the wild-type enzyme, indicating that hydrogen bond formation to an exactly positioned carbonyl oxygen plays a considerable role. The disproportionation activity is not greatly affected by the mutation because the chosen acceptor (maltotriose) only occupies subsites +1 to +3 and does not interact with the imide.

CA34 mimics the helical structure of polymeric amylose

The helical structure of CA34 in the secondary binding pocket around Y54 shows a marked similarity to an amylose helix with respect to
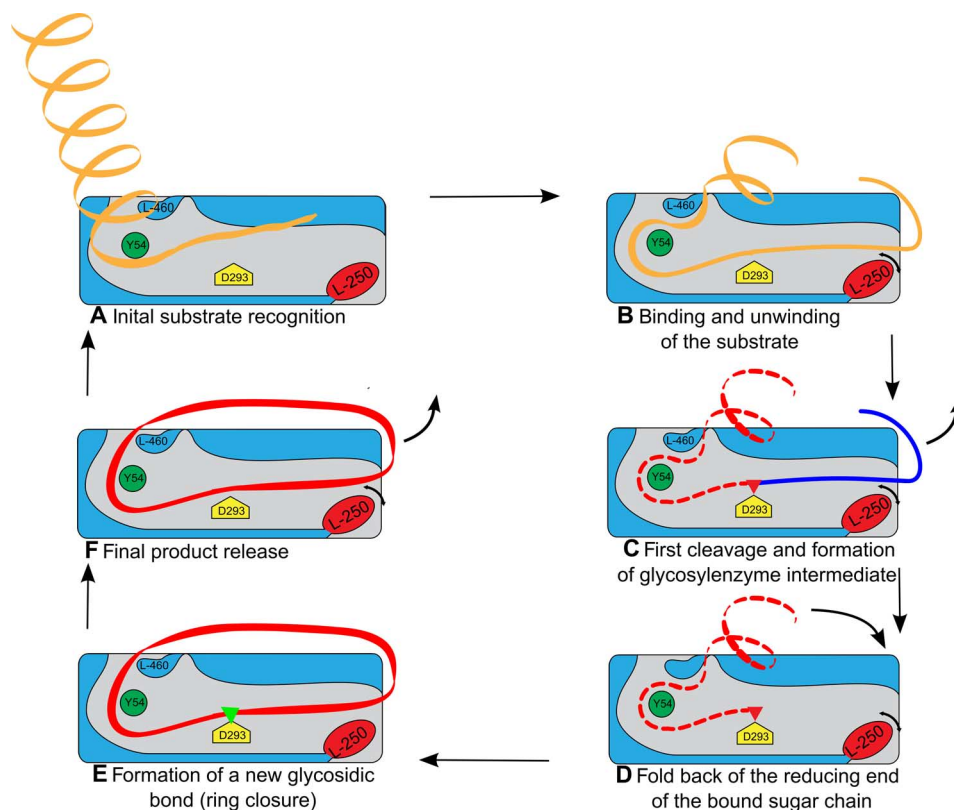
Fig. 6. Schematic catalytic cycle for CA34 formation catalyzed by AMs. (**A**) Starch amylose binds to AM at the secondary binding site in the native V-helical conformation. This binding site may thus be the site for initial substrate recognition. (**B**) The chain then protrudes into the substrate-binding crevice until all 16 subsites are filled. (**C**) After cleavage of the glycosidic bond following nucleophilic attack of D293 in the active site, the nonreducing end folds back into the acceptor site (**D**), resulting in the formation of cyclic amylose (**E**). Because of the 10 already occupied donor binding sites, the crevice defines the minimal ring size of the formed CAs, thereby acting as molecular ruler, and the two ends of the 34-glucose-long amylose are ligated at D293 to form CA34. (**F**) Release of the CA product. "L-250" and "L-460" refer to the 250 loop and 460 loop, respectively.

diameter, helical rise, and curvature (Fig. 5 and Table 1), indicating that this pocket is the initial recognition site for polymeric substrates. An equivalent region has been proposed to be also involved in the recognition of the polymeric substrate in pig pancreatic α-amylase based on the location of an α-CD ligand and further computational modeling (*14*). Mutations, destroying the sugar clamp of the secondary binding site (Y54G and Y101G mutant), lead to strongly impaired activity (Table 2). It appears that the hydrophobic platform provided by Y101 contributes mainly to the binding of polymeric substrates, whereas Y54 seems to be important as a signal element for the recognition of binding in the secondary binding site, thereby changing the conformational equilibrium of the enzyme toward a more active conformation, as suggested in previous studies (*10*) (Table 3). Likewise, a blockade of the binding path between the primary and the secondary binding site by the introduction of bulkier residues (S57R) strongly reduces AM activity (Table 2). These findings confirm the importance of the observed interactions of the whole continuous substrate-binding crevice between Y54 and the 370 loop (Fig. 1). In summary, the glucan chain is bound via 32 hydrogen bonds, 18 hydrophobic interactions, and 8 additional indirect hydrogen bonds mediated by water with a total protein-ligand interface of 1400 Å^2.

To the best of our knowledge, the structure of the complex formed between TaqAMv and CA34 presents a high-resolution representation of the interaction of polymeric amylose with AMs or related enzymes. On the basis of these results, we suggest a mode of action of AMs that

might also apply to the action of other GHs on polysaccharides in a similar way (Fig. 6, A to F).

In a first step (Fig. 6A), the helical (V-amylose) substrate docks to the initial recognition site of the enzyme around Y54 and (Fig. 6B) unwinds to bind to the catalytic crevice (with D293 as nucleophile). The flexible 250 loop adopts different positions depending on the particular function in the catalytic cycle. After chain cleavage (Fig. 6C), the former reducing end leaves the active site, and for CA formation (Fig. 6D), the nonreducing end folds back into the active site for subsequent cyclization (Fig. 6E) and product release (Fig. 6F). The extended crevice acts as a molecular ruler, defining the minimal ring size of 22 glucose moieties experimentally observed for TaqAM (*26*).

The structure of the AM-CA34 complex provides the first high-resolution structure of a carbohydrate-degrading enzyme in complex with a polymeric substrate occupying all possible subsites and reveals an initial interaction site for helical amylose. Several features are identified, which contribute to the unique reaction pattern observed for AMs, including two sugar tongs and an unusual posttranslational modification, previously only observed as an intermediate in age-related protein damage. This (previously neglected) type of modification may play a relevant role in other enzymes as a regulator of activity and substrate specificity. The unique molecular ruler feature of AMs to govern the ring size of large CA products could be rationalized on the basis of the extended substrate crevice revealed by the complex structure.

MATERIALS AND METHODS

Materials

TaqAM and all mutants were expressed and purified, as described previously for the wild-type enzyme (26). Site-directed mutagenesis was carried out as described by Weiner et al. (27). Primers for all mutations were designed accordingly, and the mutations were stepwise incorporated.

Starch hydrolysis assay

Starch-hydrolyzing activity was assayed with soluble starch as substrate by measuring the reduction of the absorption of the starch-iodine complex. The activity was assayed in 250 μl of reaction mixture containing 100 μl of 0.75% soluble starch, 100 μl of 50 mM sodium acetate (pH 5.5), and 50 μl of diluted enzyme solution. Controls contained inactivated enzyme by the addition of 500 μl of 1 M HCl. The mixture was incubated for 10 min at 70°C followed by the addition of 500 μl of 1 M HCl. A total of 100 μl of the mixture was added to 900 μl of 0.005% I_2 in 0.05% KI solution. The absorbance was measured at 660 nm, and the control value was subtracted. One unit of starch-hydrolyzing activity was defined as degradation of 1 mg of starch per minute.

Cyclization activity assay

Cyclization activity was determined by adding 5 μl of enzyme to 1345 μl of 50 mM sodium acetate buffer (pH 5.5) and 150 μl of 2% (w/v) pea starch. The reaction mixture was incubated for 90 min at 70°C. Glucoamylase (10 U) was added, and the reaction mixture was incubated at 40°C for 60 min. The mixture was centrifuged at 10,000 rpm for 15 min at room temperature, and the supernatant was analyzed by high-performance anion-exchange chromatography (HPAEC). The yield of synthesized CA25 was calculated from the peak areas of the chromatograms using CA25 as standard. One unit of cyclization activity was defined as the production of 1 mg of CA25 per minute.

Disproportionation activity assay

Disproportionation activity was determined using 30 μl of 5% (w/v) maltotriose as substrate and 20 μl of diluted enzyme solution. The mixture was incubated at 70°C for 10 min. After inactivation with 30 μl of 1 N HCl, the amount of glucose liberated from maltotriose was determined using the Glucose LiquiColor detection kit. One unit of disproportionation activity was defined as the liberation of 1 μmol of glucose per minute.

Coupling activity assay

Coupling activity was determined by incubating 0.015 mg of CA25 as donor with 0.006 mg of cellobiose as glucosyl acceptor and 10 μl of diluted enzyme solution in 370 μl of 50 mM sodium acetate buffer (pH 5.5). The mixture was incubated at 70°C for 10 min. Glucoamylase (1 U) was added, and the reaction mixture was incubated for 30 min at 40°C. The mixture was centrifuged at 10,000 rpm for 15 min at room temperature, and the supernatant was analyzed by HPAEC. The amount of residual CA25 was calculated from the peak areas of the chromatograms using CA25 as standard. One unit of coupling activity was defined as the linearization of 1 mg of CA25 per minute.

Hydrolytic activity assay

The hydrolytic activity of the AM was determined by incubating the enzyme (20 μl) with 0.0125 mg of a mixture of CA22 to CA27 for 20 min at 70°C. The enzyme was inactivated by adding 30 μl of 1 M HCl.

Reducing sugar was determined with the bicinchoninate reagent. One unit of hydrolytic activity was defined as 1 μmol of reducing sugar produced per minute.

Cocrystallization of CA with TaqAMv

A stock solution of CAs with a ring size ranging from 22 to 45 glucose units was prepared in water at a concentration of 10 mM (calculated for a mean dp of 30 for the CA mixture). The CA was produced using wild-type AM and pea starch. The resulting mixture was fractionated as described previously (28). CA stock solution was added to the protein to a final concentration of 0.1 mM. Before crystallization, the protein was dialyzed against 5 mM tris-HCl (pH 7.6), 100 mM NaCl, and 1 mM dithiothreitol and concentrated to 12 mg/ml. Initial crystallization conditions were identified using tailor-made sparse matrix screens based on commercially available screens from Hampton Research

Table 4. Data collection and refinement statistics. Values in parentheses refer to the highest-resolution shell.

	TaqAMv (D293A and D395N)
X-ray source	BL 14.2 (HZB)
Wavelength (Å)	0.91841
Space group, unit cell (Å)	I422, $a = b = 157.6$, $c = 112.8$
Resolution range (Å)	37–1.73
Completeness (%)	99.3 (99.9)
R_{merge}	0.057 (0.756)
$I/\sigma(I)$	16.9 (3.7)
Wilson B factor (Å²)	36
Redundancy	18
R/R_{free} (%)	16.40/18.84
B factor average (Å²)	51
Protein (Å²)	48
Water (Å²)	52
Carbohydrate (Å²)	81
Number of atoms	
Protein	4377
Water	443
Cycloamylose/carbohydrates	187
Ramachandran plot	
Most favored (%)	98.0
Allowed (%)	1.2
Disallowed (%)	0.8
Root mean square deviation	
Bond length (Å)	0.005
Bond angle (°)	0.807

and Jena Bioscience. Crystals suitable for x-ray diffraction were obtained by the hanging-drop vapor-diffusion method mixing 1 µl of protein per CA mix with 1 µl of reservoir containing 0.8 to 1.4 M Na/K-phosphate (pH 6.8 to 7.2). Rod-shaped crystals of space group I422 with unit cell parameters $a = b = 157.6$ Å and $c = 112.8$ Å grew within 2 weeks to a size of 200 µm × 80 µm × 80 µm. Crystals were flash-cooled in liquid nitrogen after soaking in a mixture of reservoir solution containing 0.1 mM CA as well as 30% ethanediol as cryoprotectant.

Crystallographic structure determination

Data sets were collected at beamline 14.2 at the Helmholtz-Zentrum Berlin (HZB, Germany). Data were integrated and scaled using XDS (29). Data collection parameters and statistics are provided in Table 4. The phase problem was solved by molecular replacement with the *apo* structure of TaqAM (PDB ID, 1CWY). After initial rigid body refinement, clear difference electron density for the bound CA was identified and CA34 was subsequently built up from glucose units using COOT (30). Further refinement and model building comprises alternating cycles of real space model adjustment in COOT and reciprocal refinement in Refmac and Phenix (30–32). The quality of the model was judged using MolProbity and Privateer (33, 34). The figures of molecular structures were generated with CCP4mg (35).

Accession numbers

Atomic coordinates and structure factors were deposited to the Research Collaboratory for Structural Bioinformatics PDB under accession code 5JIW.

SUPPLEMENTARY MATERIALS

Supplementary material for this article is available at http://advances.sciencemag.org/cgi/content/full/3/1/e1601386/DC1

fig. S1. Simulated annealing composite omit difference map of CA34 bound to TaqAM.

REFERENCES AND NOTES

1. V. Lombard, H. Golaconda Ramulu, E. Drula, P. M. Coutinho, B. Henrissat, The carbohydrate-active enzymes database (CAZy) in 2013. *Nucleic Acids Res.* **42**, D490–D495 (2014).
2. I. Przylas, K. Tomoo, Y. Terada, T. Takaha, K. Fujii, W. Saenger, N. Sträter, Crystal structure of amylomaltase from *Thermus aquaticus*, a glycosyltransferase catalysing the production of large cyclic glucans. *J. Mol. Biol.* **296**, 873–886 (2000).
3. K. L. Larsen, Large cyclodextrins. *J. Incl. Phenom. Macrocycl. Chem.* **43**, 1–13 (2002).
4. O. Nimz, K. Geßler, I. Usón, S. Laettig, H. Welfle, G. M. Sheldrick, W. Saenger, X-ray structure of the cyclomaltohexaicosaose triiodide inclusion complex provides a model for amylose–iodine at atomic resolution. *Carbohydr. Res.* **338**, 977–986 (2003).
5. O. Nimz, K. Gessler, I. Usón, G. M. Sheldrick, W. Saenger, Inclusion complexes of V-amylose with undecanoic acid and dodecanol at atomic resolution: X-ray structures with cycloamylose containing 26 D-glucoses (cyclohexaicosaose) as host. *Carbohydr. Res.* **339**, 1427–1437 (2004).
6. W. Saenger, J. Jacob, K. Gessler, T. Steiner, D. Hoffmann, H. Sanbe, K. Koizumi, S. M. Smith, T. Takaha, Structures of the common cyclodextrins and their larger analogues—Beyond the doughnut. *Chem. Rev.* **98**, 1787–1802 (1998).
7. S. Machida, S. Ogawa, S. Xiaohua, T. Takaha, K. Fujii, K. Hayashi, Cycloamylose as an efficient artificial chaperone for protein refolding. *FEBS Lett.* **486**, 131–135 (2000).
8. T. R. M. Barends, J. B. Bultema, T. Kaper, M. J. E. C. van der Maarel, L. Dijkhuizen, B. W. Dijkstra, Three-way stabilization of the covalent intermediate in amylomaltase, an α-amylase-like transglycosylase. *J. Biol. Chem.* **282**, 17242–17249 (2007).
9. I. Przylas, Y. Terada, K. Fujii, T. Takaha, W. Saenger, N. Sträter, X-ray structure of acarbose bound to amylomaltase from *Thermus aquaticus*. Implications for the synthesis of large cyclic glucans. *Eur. J. Biochem.* **267**, 6903–6913 (2000).
10. T. Kaper, H. Leemhuis, J. C. M. Uitdehaag, B. A. van der Veen, B. W. Dijkstra, M. J. E. C. van der Maarel, L. Dijkhuizen, Identification of acceptor substrate binding subsites +2 and +3 in the amylomaltase from *Thermus thermophilus* HB8. *Biochemistry* **46**, 5261–5269 (2007).
11. J. C. M. Uitdehaag, K. H. Kalk, B. A. van der Veen, L. Dijkhuizen, B. W. Dijkstra, The cyclization mechanism of cyclodextrin glycosyltransferase (CGTase) as revealed by a γ-cyclodextrin-CGTase complex at 1.8-Å resolution. *J. Biol. Chem.* **274**, 34868–34876 (1999).
12. C. Christiansen, M. Abou Hachem, S. Janecek, A. Viksø-Nielsen, A. Blennow, B. Svensson, The carbohydrate-binding module family 20—Diversity, structure, and function. *FEBS J.* **276**, 5006–5029 (2009).
13. D. Guillén, S. Sánchez, R. Rodríguez-Sanoja, Carbohydrate-binding domains: Multiplicity of biological roles. *Appl. Microbiol. Biotechnol.* **85**, 1241–1249 (2010).
14. S. B. Larson, J. S. Day, A. McPherson, X-ray crystallographic analyses of pig pancreatic α-amylase with limit dextrin, oligosaccharide, and α-cyclodextrin. *Biochemistry* **49**, 3101–3115 (2010).
15. A. Cheng, M. Zhang, K. Okubo, K. Omichi, A. R. Saltiel, Distinct mutations in the glycogen debranching enzyme found in glycogen storage disease type III lead to impairment in diverse cellular functions. *Hum. Mol. Genet.* **18**, 2045–2052 (2009).
16. E. C. O'Neill, C. E. M. Stevenson, K. Tantanarat, D. Latousakis, M. I. Donaldson, M. Rejzek, S. A. Nepogodiev, T. Limpaseni, R. A. Field, D. M. Lawson, Structural dissection of the maltodextrin disproportionation cycle of the *Arabidopsis* plastidial disproportionating enzyme 1 (DPE1). *J. Biol. Chem.* **290**, 29834–29853 (2015).
17. T. Geiger, S. Clarke, Deamidation, isomerization, and racemization at asparaginyl and aspartyl residues in peptides. Succinimide-linked reactions that contribute to protein degradation. *J. Biol. Chem.* **262**, 785–794 (1987).
18. S. Noguchi, K. Miyawaki, Y. Satow, Succinimide and isoaspartate residues in the crystal structures of hen egg-white lysozyme complexed with tri-N-acetylchitotriose. *J. Mol. Biol.* **278**, 231–238 (1998).
19. S. Noguchi, Structural changes induced by the deamidation and isomerization of asparagine revealed by the crystal structure of *Ustilago sphaerogena* ribonuclease U2B. *Biopolymers* **93**, 1003–1010 (2010).
20. A. E. Roher, J. D. Lowenson, S. Clarke, C. Wolkow, R. Wang, R. J. Cotter, I. M. Reardon, H. A. Zürcher-Neely, R. L. Heinrikson, M. J. Ball, B. D. Greenberg, Structural alterations in the peptide backbone of β-amyloid core protein may account for its deposition and stability in Alzheimer's disease. *J. Biol. Chem.* **268**, 3072–3083 (1993).
21. N. Fujii, Y. Ishibashi, K. Satoh, M. Fujino, K. Harada, Simultaneous racemization and isomerization at specific aspartic acid residues in αB-crystallin from the aged human lens. *Biochim. Biophys. Acta* **1204**, 157–163 (1994).
22. N. Fujii, K. Satoh, K. Harada, Y. Ishibashi, Simultaneous stereoinversion and isomerization at specific aspartic acid residues in αA-crystallin from human lens. *J. Biochem.* **116**, 663–669 (1994).
23. E. Kim, J. D. Lowenson, D. C. MacLaren, S. Clarke, S. G. Young, Deficiency of a protein-repair enzyme results in the accumulation of altered proteins, retardation of growth, and fatal seizures in mice. *Proc. Natl. Acad. Sci. U.S.A.* **94**, 6132–6137 (1997).
24. S. Eschenburg, E. Schönbrunn, Comparative X-ray analysis of the un-liganded fosfomycin-target murA. *Proteins* **40**, 290–298 (2000).
25. C. L. David, J. Keener, D. W. Aswad, Isoaspartate in ribosomal protein S11 of *Escherichia coli*. *J. Bacteriol.* **181**, 2872–2877 (1999).
26. Y. Terada, K. Fujii, T. Takaha, S. Okada, *Thermus aquaticus* ATCC 33923 amylomaltase gene cloning and expression and enzyme characterization: Production of cycloamylose. *Appl. Environ. Microbiol.* **65**, 910–915 (1999).
27. M. P. Weiner, G. L. Costa, W. Schoettlin, J. Cline, E. Mathur, J. C. Bauer, Site-directed mutagenesis of double-stranded DNA by the polymerase chain reaction. *Gene* **151**, 119–123 (1994).
28. M. N. Mokhtar, K. U. Lauckner, W. Zimmermann, U.S. Patent EP2223942A1 (2010).
29. W. Kabsch, XDS. *Acta Crystallogr. Sect. D Biol. Crystallogr.* **66** (Pt. 2), 125–132 (2010).
30. P. Emsley, B. Lohkamp, W. G. Scott, K. Cowtan, Features and development of *Coot*. *Acta Crystallogr. Sect. D Biol. Crystallogr.* **66**, 486–501 (2010).
31. P. D. Adams, P. V. Afonine, G. Bunkóczi, V. B. Chen, N. Echols, J. J. Headd, L.-W. Hung, S. Jain, G. J. Kapral, R. W. Grosse Kunstleve, A. J. McCoy, N. W. Moriarty, R. D. Oeffner, R. J. Read, D. C. Richardson, J. S. Richardson, T. C. Terwilliger, P. H. Zwart, The Phenix software for automated determination of macromolecular structures. *Methods* **55**, 94–106 (2011).
32. G. N. Murshudov, P. Skubák, A. A. Lebedev, N. S. Pannu, R. A. Steiner, R. A. Nicholls, M. D. Winn, F. Long, A. A. Vagin, REFMAC5 for the refinement of macromolecular crystal structures. *Acta Crystallogr. Sect. D Biol. Crystallogr.* **67**, 355–367 (2011).
33. V. B. Chen, W. B. Arendall III, J. J. Headd, D. A. Keedy, R. M. Immormino, G. J. Kapral, L. W. Murray, J. S. Richardson, D. C. Richardson, MolProbity: All-atom structure validation for macromolecular crystallography. *Acta Crystallogr. Sect. D Biol. Crystallogr.* **66**, 12–21 (2010).

34. J. Agirre, J. Iglesias-Fernández, C. Rovira, G. J. Davies, K. S. Wilson, K. D. Cowtan, Privateer: Software for the conformational validation of carbohydrate structures. *Nat. Struct. Mol. Biol.* **22**, 833–834 (2015).

35. S. McNicholas, E. Potterton, K. S. Wilson, M. E. Noble, Presenting your structures: The CCP4mg molecular-graphics software. *Acta Crystallogr. Sect. D Biol. Crystallogr.* **67**, 386–394 (2011).

36. K. Gessler, I. Usón, T. Takaha, N. Krauss, S. M. Smith, S. Okada, G. M. Sheldrick, W. Saenger, V-Amylose at atomic resolution: X-ray structure of a cycloamylose with 26 glucose residues (cyclomaltohexaicosaose). *Proc. Natl. Acad. Sci. U.S.A.* **96**, 4246–4251 (1999).

Citation: C. Roth, N. Weizenmann, N. Bexten, W. Saenger, W. Zimmermann, T. Maier, N. Sträter, Amylose recognition and ring-size determination of amylomaltase. *Sci. Adv.* **3**, e1601386 (2017).